Basic & Clinical Pharmacology & Toxicology

BCPT Basic & Clinical Pharmacology & Toxicology

ORIGINAL ARTICLE OPEN ACCESS

Increased Mitochondrial Superoxide Level Is Partially Associated With Vemurafenib-Induced Renal Tubular Toxicity

Akimasa Sanagawa[1] | Hiroshi Takase[2]

[1]Department of Clinical Pharmaceutics, Nagoya City University Graduate School of Medical Sciences, Nagoya, Japan | [2]Research Equipment Sharing Center, Nagoya City University Graduate School of Medical Sciences, Nagoya, Japan

Correspondence: Akimasa Sanagawa (phsanag@med.nagoya-cu.ac.jp)

Received: 24 October 2024 | **Revised:** 12 February 2025 | **Accepted:** 19 February 2025

Funding: This work was supported by grants from the Public Foundation of Chubu Science and Technology Center, Aichi Cancer Research Foundation and JSPS KAKENHI (19K16417, 21K15319 and 23K06257) to A.S.

Keywords: lysosomal abnormalities | mitochondrial dysfunction | renal tubular toxicity | superoxide | vemurafenib

ABSTRACT

Vemurafenib (VEM) reportedly inhibits the mitochondrial respiratory chain and reduces ferrochelatase (FECH) activity, thereby causing VEM-induced renal tubular toxicity. However, the exact mechanisms underlying VEM-induced renal tubular toxicity remain unclear. In this study, we treated human renal proximal tubular epithelial cells with VEM to elucidate these mechanisms. VEM treatment for 24 h resulted in cell damage, reduced cell viability, increased lactate dehydrogenase release and elevated the production of inflammatory cytokines. Transmission electron microscopy (TEM) and fluorescence microscopy revealed accumulation and enlargement of lysosome-derived vacuoles and mitochondrial superoxide production. Although MitoTracker showed no change in the total mitochondrial volume, TEM indicated mitochondrial damage, including smaller and less visible mitochondria. Enhanced superoxide production was confirmed using mtSOX. The mitochondria-specific antioxidant XJB-5-131 partially alleviated VEM-induced superoxide production and improved cell viability, indicating the role of superoxide in VEM-induced renal tubular toxicity. The inhibition of lysosomal acidification by bafilomycin A1 did not mitigate VEM-induced cytotoxicity, suggesting potential autophagy impairment. These findings highlight that mitochondrial dysfunction and lysosomal abnormalities are significant factors in VEM-induced renal tubular toxicity, warranting further investigation into the relationship between their mechanisms, reduced FECH activity and potential renoprotective targets.

1 | Introduction and Background

Patients undergoing anticancer therapy can often develop acute kidney injury (AKI) [1–4]. Over the past decades, numerous anticancer drugs including conventional cytotoxic agents, targeted antibodies and small-molecule agents have received approval worldwide [5, 6]. However, these drugs are known to be nephrotoxic [1–3, 7]. Vemurafenib (VEM) is a first-generation inhibitor of v-Raf murine sarcoma viral oncogene homologue B1 (BRAF), a major oncogenic driving factor. Clinical trials on VEM have reported that it can lead to the development of secondary cutaneous squamous-cell carcinoma but have not reported renal adverse events [8, 9]. Postmarketing, several studies have reported that VEM is associated with an increased risk of developing AKI [10–13]. It is possible that VEM-induced renal adverse events involve a dual mechanism, inhibition of creatinine tubular secretion and slight impairment of renal function, leading to an increase in plasma creatinine levels [14].

Summary

- Vemurafenib (VEM), an anticancer drug, reportedly causes VEM-induced renal tubular toxicity.
- We treated human renal proximal tubular epithelial cells with VEM to elucidate the mechanisms of its effects.
- VEM treatment resulted in cell damage, reduced cell viability, increased lactate dehydrogenase release and elevated the production of inflammatory cytokines.
- Lysosome-derived vacuoles were large and accumulated, mitochondrial superoxide was produced, and mitochondria were damaged.
- The mitochondria-specific antioxidant XJB-5-131 partially alleviated the superoxide production and improved cell viability, indicating that superoxide plays a role in VEM-induced renal tubular toxicity.
- Mitochondrial dysfunction and lysosomal abnormalities are significant factors in VEM-induced renal tubular toxicity.

Bai et al. shed some light on the mechanism underlying VEM-induced renal tubular toxicity by focusing on ferrochelatase (FECH), the final enzyme in heme synthesis localised in the mitochondria [15]. They established an AKI mouse model by inducing VEM renal toxicity and demonstrated that BRAF, the primary target of VEM, is not involved in VEM-induced renal tubular toxicity; instead, the mechanism involves the off-target effect of FECH inhibition [15]. Moreover, they found that AKI develops 2 weeks after VEM administration and that RNA knockdown or loss-of-function mutation in FECH accelerates the onset of VEM-induced AKI. On the other hand, overexpression of FECH in cultured renal tubule cells can prevent VEM-induced cell death. These pharmacological and genetic inhibition experiments concluded that the decrease in FECH activity caused by VEM is partially involved in renal tubular toxicity [15].

Erythropoietic protoporphyria is an inherited metabolic disorder caused by a deficiency of FECH [16–18]. Although the liver and bone marrow are the primary organs for heme synthesis, the kidney also has the ability to synthesise heme, which is localised within proximal tubular cells [19, 20]. The main symptoms of erythropoietic protoporphyria are cutaneous photosensitivity and liver dysfunction, and not tubular injury [16–18]. However, tubular injury has been reported in acute intermittent porphyria characterised by abnormalities in hydroxymethylbilane synthase, another enzyme involved in heme synthesis [21, 22]. Therefore, it appears that a decrease in FECH activity does not directly lead to tubular injury. These fundamental experimental findings and clinical observations suggest that mechanisms other than FECH inhibition contribute to VEM-induced renal tubular toxicity.

Therefore, the present study aimed to investigate the mechanism underlying VEM-induced renal toxicity with a focus on the cellular ultrastructure and function of intracellular organelles in renal tubular epithelial cells. We found that VEM induces lysosomal and mitochondrial dysfunctions, and mitochondrial-specific antioxidants alleviate VEM-induced renal tubular toxicity. These findings highlight a potential pathway contributing to VEM-induced renal injury.

2 | Materials and Methods

The study was conducted in accordance with the Basic & Clinical Pharmacology & Toxicology policy for experimental and clinical studies [23].

2.1 | Cell Culture

Human renal proximal tubule epithelial cells (RPTECs), purchased from Lonza (Basal, Switzerland), were cultured in REGM Renal Epithelial Cell Growth Medium BulletKit (Lonza), following previously described methods [24, 25]. In this study, RPTECs from Passages 4–8 were used to avoid the effects of replicative-induced cellular senescence [25].

2.2 | Chemicals

VEM (Cat #S1267; Selleck Chemicals, Houston, TX, USA), bafilomycin A1 (BAFA1) (Cell Signaling Technology, Cat #54645) and XJB-5-131 (Sigma-Aldrich, Cat #SML2982) were dissolved in dimethyl sulfoxide (DMSO) (Fujifilm Wako). Cisplatin (Fujifilm Wako Chemicals, Cat #C499500) was dissolved in REGM Renal Epithelial Cell Growth Medium BulletKit. When only VEM was added to the medium, the solution was diluted to achieve a DMSO concentration of 0.1%. When VEM and the other compounds were added simultaneously to the medium, the solution was diluted to achieve a DMSO concentration of 0.2%. All chemicals used for analyses were of analytical grade or higher.

2.3 | Cell Viability Assay

RPTECs were seeded in 96-well plates at a density of 7×10^3 cells/well and incubated for 24 h. VEM at different concentrations was then added to the cells by changing the medium in the plates to a culture medium containing the drug. Cell viability was assessed using the Cell Counting Kit 8 (CCK-8) (Dojindo Laboratories, Kumamoto, Japan), as previously reported [23]. The cells were incubated before adding aliquots of 10-μL CCK-8 solution to each well. Following this, incubation was continued for 2 h, and the absorbance was measured at 450 nm using a SpectraMax iD3 multi-mode microplate reader (Molecular Devices, Osaka, Japan). The percentage of cell viability in the drug-treated samples relative to that in the corresponding drug-naïve samples was calculated.

2.4 | Lactate Dehydrogenase Release Assay

Components of Cytotoxicity Lactate Dehydrogenase (LDH) Assay Kit-WST (Dojindo Laboratories) were used to detect cell death or cell damage, following previously described procedures

[24]. The cells were incubated either as controls or with VEM at various concentrations for 22 h. Subsequently, one set of control cells (maximum control) was treated with 20-μL lysis buffer, and the mixture was incubated for 30 min. Supernatant aliquots of 100 μL were obtained from the wells of the cell culture plate and transferred to the wells of a 96-well LDH assay plate. The plate was incubated for 30 min at room temperature (25°C) in dark conditions. Stop solution aliquots of 50 μL were then added to each well of the assay plate, and absorbance was measured at 490 nm using the SpectraMax iD3 multi-mode microplate reader (Molecular Devices). The percentage of LDH released in the test samples relative to that in the maximum control samples was calculated.

2.5 | Apoptosis and Necrosis Assay

Apoptosis and necrosis were assessed using the RealTime-Glo Annexin V Apoptosis and Necrosis Assay kit (Promega, Walldorf, Germany), according to the manufacturer's instructions. Cells were seeded in a 96-well white-bottom plate at a density of 1×10^4 cells/well. VEM was diluted in the medium and added in 100-μL volumes. Untreated cells in the medium served as the control. Next, 100 μL of the 2× detection reagent, containing 12-mL medium, 24-μL Annexin NanoBit substrate, 24-μL $CaCl_2$, 24-μL necrosis detection reagent, 24-μL Annexin V-SmBiT and 24-μL Annexin V-LgBiT, was added to each well. The plate was shaken for 5 s, and both luminescence and fluorescence were measured after 24 h using a Spectra Max iD3 multi-mode microplate reader (Molecular Devices). The excitation and emission wavelengths were set to 488 and 530 nm, respectively.

2.6 | Real-Time Quantitative PCR (qPCR)

qPCR analysis was performed as previously reported [25]. Briefly, total RNA was extracted from the RPTECs of each passage using the PureLink RNA Mini Kit (Thermo Fischer Scientific, Waltham, MA, USA), according to the manufacturer's instructions. Using ReverTra qPCR RT Master Mix with gDNA Remover (Toyobo Co., Ltd., Osaka, Japan), total RNA was reverse-transcribed into cDNA. Subsequently, PCR was performed using the PowerUp SYBR Green Master Mix (Thermo Fischer Scientific). The primers used in the experiment are listed in Table 1. For detecting damage and inflammation in RPTECs, primer pairs for kidney injury molecule (KIM)-1 and representative inflammation markers, namely, monocyte chemotactic protein (MCP)-1, interleukin (IL)-6, IL-8, tumour necrosis factor (TNF)α, IL-1α and transforming growth factor (TGF)β, were designed [26–30]. Amplification and detection were performed using the CFX Connect Real-Time System (Bio-Rad Laboratories Inc., Hercules, CA, USA). *ACTB* was used as the endogenous control, and mRNA levels were quantified using the ΔΔCt method. All measurements were performed in triplicate. The mRNA levels of renal tubule damage and inflammation markers were expressed as fold changes relative to the control.

2.7 | Transmission Electron Microscopy (TEM)

For TEM, samples were fixed in 2% glutaraldehyde (Nisshin-EM, Cat #3055-1) and 0.1-M phosphate buffer (pH 7.4). The cells were then treated with 2% OsO_4 (Nisshin-EM, Cat #3020-4) in the same buffer. Fixed specimens were washed, dehydrated in a graded series of ethanol and embedded in Quetol 812 epoxy

TABLE 1 | Primer pairs for quantitative real-time PCR.

Protein (gene) name	NCBI ref. seq.	Direction	Sequence
KIM-1 (KIM-1)	NM_012206	Forward	5′-CAGAACCATGAACCAGTAGCCA-3′
		Reverse	5′-GTGAGCTGGTGGGTTCTCTC-3′
MCP-1 (MCP-1)	NM_002982	Forward	5′-TCCCAAAGAAGCTGTGATCTTCA-3′
		Reverse	5′-TCTGGGGAAAGCTAGGGGAA-3′
IL-6 (IL-6)	NM_000600	Forward	5′-AGAGGCACTGGCAGAAAACA-3′
		Reverse	5′-TCACCAGGCAAGTCTCCTCA-3′
IL-8 (IL-8)	NM_000584	Forward	5′-TCAGAGACAGCAGAGCACAC-3′
		Reverse	5′-CTTGGCAAAACTGCACCTTCA-3′
TNFα (TNFA)	NM_000594	Forward	5′-GTAGCCCATGTTGTAGCAAACC-3′
		Reverse	5′-TATCTCTCTCAGCTCCACGCCA-3′
IL-1α (IL-1A)	NM_000575	Forward	5′-AATGATCAGTACCTCACGGCTG-3′
		Reverse	5′-TATCTCAGGCATCTCCTTCAGCA-3′
TGFβ (TGFB)	MN_000660	Forward	5′-CAAGTGGACATCAACGGGTTC-3′
		Reverse	5′-ATGAGAAGCAGGAAAGGCCG-3′
ACTβ (ACTB)	NM_001101	Forward	5′-GATTCCTATGTGGGCGACGA-3′
		Reverse	5′-AGGTCTCAAACATGATCTGGGT-3′

Note: List of all primer sequences including their NCBI ref. seq. numbers.

resin (Nisshin-EM, Cat #348) for 24 h at 60°C to ensure polymerisation [31]. Ultra-thin sections (90–100 nm) were cut using Ultracut UCT (Leica) with a diamond knife and then stained with 2% uranyl acetate in distilled water for 15 min and with modified Sato's lead solution for 5 min [32]. The sections were analysed using a JEM-1400Plus transmission electron microscope (JEOL, Tokyo, Japan). To compare the effects of VEM with those of a well-characterised nephrotoxin, cisplatin was used as a positive control.

2.8 | Fluorescence Microscope Imaging and Quantification Analysis

Cells were seeded in 35-mm glass bottom dishes coated with poly-lysine (Matsunami Glass Ind., Osaka, Japan) at a density of 5×10^4 cells and returned to the incubator for 24 h. The cells were then incubated with a medium containing 50-nM MitoTracker Green FM (Invitrogen, Carlsbad, CA, USA), 50-nM LysoTracker Deep Red (Invitrogen) and 0.1% of 1-mg/mL Hoechst 33342 (Dojindo Laboratories) for 30 min. Subsequently, cells were washed two times using Hank's balanced salt solution (HBSS) with *N*-(2-hydroxyethyl)piperazine-*N*′-2-ethanesulphonic acid (HEPES) (Bio Medical Science, Tokyo, Japan). Next, cells were incubated with a medium containing 0.1% DMSO as control, 50-nM BAFA1 or 50-μM VEM for 24 h. MitoTracker, LysoTracker and Hoechst 33342 images were obtained using an all-in-one fluorescence microscope (BZ-X810; KEYENCE, Osaka, Japan) with a Plan Fluorite 20× LD PH objective (NA0.45, BZ-PF20LP; KEYENCE). Green fluorescence of MitoTracker was detected using a GFP filter (excitation: 470/40 nm, emission: 525/50 nm, dichroic mirror: 495 nm; OP-87763; KEYENCE). Red fluorescence of LysoTracker Deep Red was detected using a Cy5 filter (excitation: 620/60 nm, emission: 700/75 nm, dichroic mirror: 660 nm; OP-87766; KEYENCE). Blue fluorescence of Hoechst 33342 was detected using a DAPI filter (excitation: 360/40 nm, emission: 460/50 nm, dichroic mirror: 400 nm; OP-87762; KEYENCE). The mean relative fluorescence intensity of MitoTracker and LysoTracker per cell in the control group was set to 100. The cell number was determined by the number of nuclei stained with Hoechst 33342. Superoxide images were obtained using BZ-X810 with a Plan Fluorite 10× LD PH objective (NA0.30, BZ-PF10P; KEYENCE). The red fluorescence of mtSOX Deep Red (Dojindo Laboratories), an indicator of superoxide, was detected using a Texas Red filter (excitation: 560/40 nm, emission: 630/75 nm, dichroic mirror: 585 nm; OP-87765; KEYENCE). The mean relative fluorescence intensity of mtSOX Deep Red in the control group or VEM + DMSO group was set to 100. Four images were randomly selected from each group, and the signal intensities of MitoTracker, LysoTracker and mtSOX Deep Red were automatically calculated using the hybrid cell count application BZ-H4A in the BZ-X Analyzer Software BZ-H4A [33]. The values of signal intensities per cell were calculated by dividing by the number of Hoechst 33342-stained nuclei.

2.9 | Time-Lapse Imaging of Mitochondrial Superoxide Product

Following the uptake of mtSOX Deep Red for 30 min and two washes with HBSS, the medium was replaced with a medium containing DMSO, VEM, VEM + DMSO or VEM + XJB-5-131. Time-lapse images were obtained at 15-min intervals for 24 h using the all-in-one fluorescence microscope BZ-X810 (KEYENCE) equipped with the time-lapse module BZ-H4XT and a stage-top chamber and temperature controller with the built-in CO_2 gas mixer INUG2-KIW (Tokai hit, Shizuoka, Japan) at 37°C and 5% CO_2. Superoxide images were obtained using BZ-X810 with a Plan Fluorite 10× LD PH objective. The signal intensity of mtSOX Deep Red was automatically calculated using the hybrid cell count application BZ-H4A in the BZ-X Analyzer Software BZ-H4A [34]. When comparing the two groups, the relative fluorescence intensity of mtSOX Deep Red at the start of the observation in the group with lower values was set to 1, and the change in fluorescence over time was plotted on an X-Y graph.

2.10 | Statistical Analysis

Data are expressed as mean ± standard deviation. To determine the statistical significance between two groups, we first performed the Shapiro–Wilk test and equal variance test. If the assumptions of both tests were validated, we applied an unpaired *t*-test. If the data did not show a normal distribution, we applied the Mann–Whitney *U* test; if the data did not exhibit equal variance, Welch's *t*-test was used. Multiple comparisons between the control and other groups were performed using one-way ANOVA with Dunnett's multiple comparison test. The Kruskal–Wallis test was performed to compare three or more groups. $p < 0.05$ was considered to indicate a statistically significant difference. All statistical analyses were performed using SPSS (version 23.0; IBM SPSS Inc., Tokyo, Japan). Figures were generated using GraphPad Prism (version 9; GraphPad Software, Boston, MA, USA).

3 | Results

3.1 | VEM-Induced Cytotoxicity and Intracellular Ultrastructure Changes in Human RPTECs

To determine VEM cytotoxicity in primary human RPTECs, we evaluated cell viability using the CCK-8 assay (Figure 1A). Dunnett's multiple comparison test revealed significant differences at VEM concentrations of 1 μM and above compared with 0 μM ($p < 0.01$; one-way ANOVA with Dunnett's multiple comparison test). Subsequently, cellular damage assessment using the LDH assay revealed a dose-dependent increase in LDH release due to VEM exposure (Figure 1B). Based on previous findings, the concentration of VEM selected for subsequent experiments was 50 μM [15]. The exposure time was 24 h. In the apoptosis and necrosis assays, compared with the control, VEM did not induce changes in apoptosis-like cell death but increased necrosis-like cell death (Figure 1C,D). Additionally, the mRNA levels of KIM-1, MCP-1, IL-6, IL-8, TNFα, IL-1α and TGFβ exhibited a concomitant increase with VEM exposure. The levels of these mRNAs, compared with the control, increased by 1.53 ± 0.11 times ($p = 0.001$ by Welch's *t*-test), 5.08 ± 1.73 times ($p = 0.004$ by unpaired *t*-test), 1.64 ± 0.66 times ($p = 0.343$ by Mann–Whitney *U* test), 46.23 ± 29.21 times ($p = 0.010$ by unpaired *t*-test), 6.19 ± 1.17

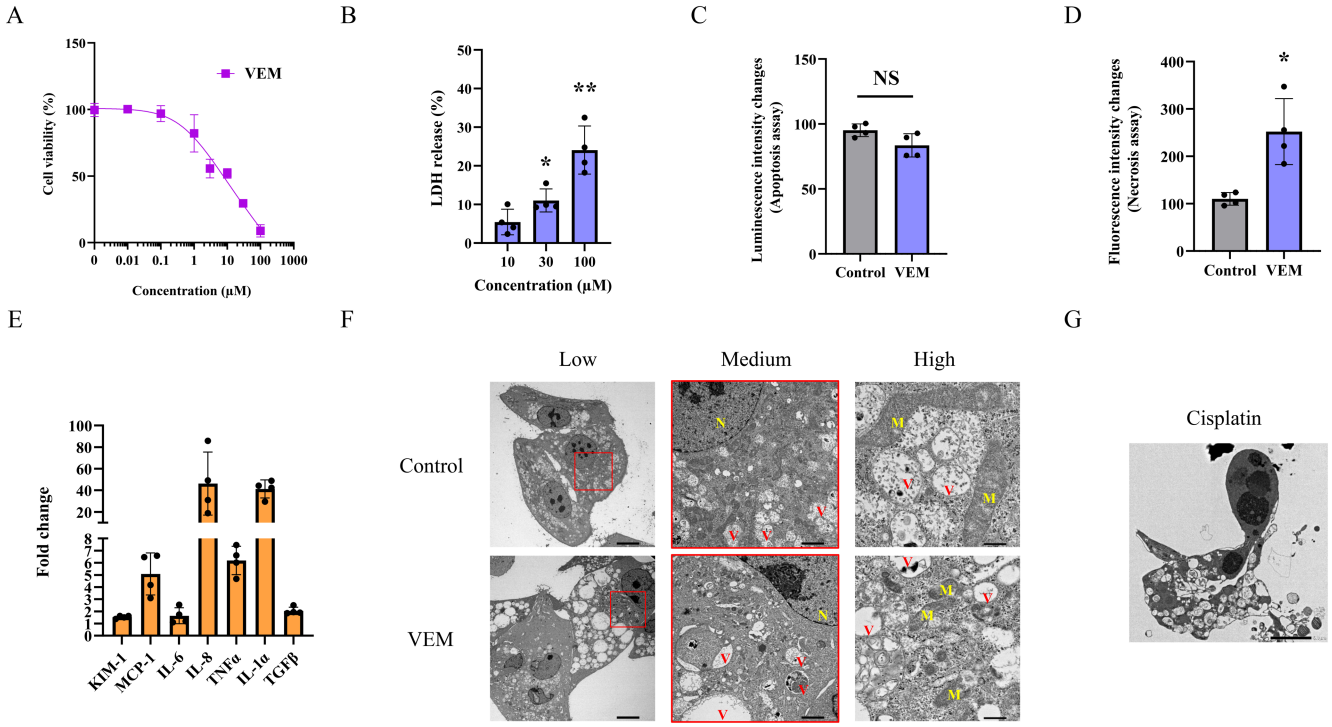

FIGURE 1 | Vemurafenib (VEM)-induced cytotoxicity and changes in intracellular ultrastructure in human renal proximal tubule epithelial cells (RPTECs). RPTECs were treated with vehicle or VEM for 24 h. (A) Cell viability was determined using the CCK-8 assay ($n = 4$) (B) Cell damage was determined using the lactate dehydrogenase (LDH) assay (*$p < 0.05$, **$p < 0.01$ compared with 10-μM VEM; one-way ANOVA with Dunnett's multiple comparison test). (C and D) Quantitative results of apoptosis and necrosis analysed using luminescence and fluorescence intensity (*$p < 0.05$; Welch's t-test) ($n = 4$). (E) VEM-induced change of mRNA expression levels of KIM-1, MCP-1, IL-6, IL-8, TNFα, IL-1α and TGFβ in RPTECs exposed to 50-μM VEM compared with vehicle for 24 h ($n = 4$). (F) TEM showing VEM-induced changes in the intracellular ultrastructure of RPTECs. N, nucleoli; M, mitochondria; V, vacuoles. The area outlined by the square in the low-magnification image is shown at a higher magnification in the medium-magnification image. Low magnification 500× (scale bar, 10 μm); medium magnification 2500× (scale bar, 2 μm); high magnification 10000× (scale bar, 500 nm). (G) TEM image of typical apoptosis in RPTEC exposed to 50-μM cisplatin for 24 h (magnification: 1500×; scale bar, 5 μm). Data are presented as the mean ± standard deviation. $p < 0.05$ indicates statistical significance. NS, not significant.

times ($p < 0.001$ by unpaired t-test), 41.28 ± 8.30 times ($p < 0.001$ by unpaired t-test) and 2.04 ± 0.30 times ($p < 0.001$ by unpaired t-test), respectively (Figure 1E).

TEM ultrastructure analysis provided additional insights into VEM-induced cytotoxicity in RPTECs (Figure 1F). At low magnification, an increase in the number of vacuoles, along with their enlargement, and the presence of irregularly shaped nuclei were observed. At medium-to-high magnification, the enlarged vacuoles were observed to contain cellular debris, speculated to be derived from dysfunctional lysosomes. Under VEM treatment, most mitochondria that were visible under control conditions became less visible and smaller in size. No changes in cell membrane integrity or necrosis-like cell death were observed. The cell microstructure of RPTECs exposed to 50-μM cisplatin, used as a positive control of apoptosis, was observed at 24 h (Figure 1G), revealing fragmented nuclei, condensed chromatin and apoptotic bodies. These typical features of apoptosis were not observed in most RPTECs exposed to 50-μM VEM for 24 h, suggesting that these were damaged prior to cell death.

Hino et al. reported expanded vacuoles derived from lysosomes, similar to that observed during abemaciclib-induced atypical cell death in cancer cells [35]. Additionally, mitochondrial size and shape are regulated by fission and fusion [36, 37]. Ischemic- and cisplatin-induced renal injury exhibits mitochondrial fission, and genetic and pharmacological deletion of mitochondrial fission accelerates kidney function recovery [36, 37]. This is an important phenomenon related to mitochondrial damage, renal tubule damage or cell death [36, 37]. Based on these results, we further examined the effects of VEM on expanded vacuoles and mitochondria.

3.2 | VEM Induces Lysosome Abnormalities and Mitochondrial Superoxide Production in Human RPTECs

MitoTracker- and LysoTracker-based fluorescent staining was used to analyse the effects of VEM on mitochondria and lysosome-like vacuoles. VEM exposure did not significantly affect the fluorescence intensity of the mitochondria, suggesting that VEM had little effect on the volume or integrity of mitochondria within 24 h (Figure 2A,B). In contrast, the fluorescence intensity of the lysosomes significantly increased following VEM exposure (Figure 2A,C). BAFA1, an inhibitor of vacuolar-type ATPase that inhibits acidification in the lysosomes of cultured cells [38], induced a loss of LysoTracker fluorescence (Figure 2A,C), confirming that LysoTracker can effectively track lysosomes. These results were consistent with the increase

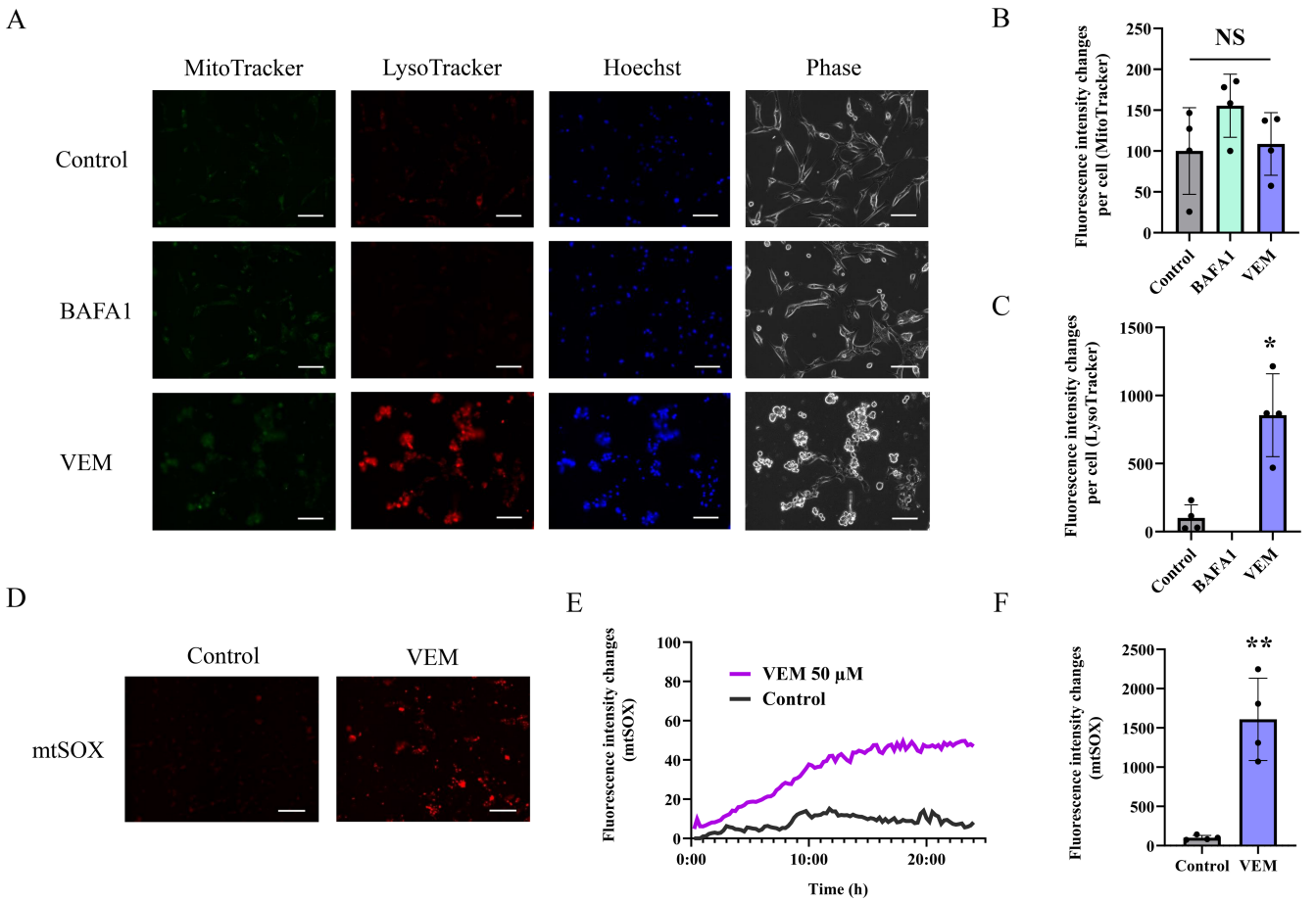

FIGURE 2 | VEM induces lysosome abnormalities and mitochondrial superoxide production in human RPTECs. (A) LysoTracker can identify vacuoles derived from lysosome. LysoTracker fluorescence microscopy showed a decrease in fluorescence intensity by BAFA1 and an increase in fluorescence intensity by VEM. Representative images of four independent experiments. Images captured using a 20× objective lens. Scale bar, 100 μm. (B) VEM and BAFA1 did not affect relative changes in fluorescence intensity of MitoTracker per cell ($p = 0.232$; Kruskal–Wallis test) ($n = 4$). (C) BAFA1 reduced fluorescence of LysoTracker. VEM induced a significant increase in the relative change in fluorescence intensity of LysoTracker per cell (*$p < 0.05$; Welch's t-test) ($n = 4$). (D) mtSOX is oxidised by mitochondrial superoxide and accumulates in mitochondria. mtSOX fluorescence signals increased in RPTECs treated with 50-μM VEM for 24 h. Images captured using a 10× objective lens. Scale bar, 200 μm. (E) Time-lapse fluorescence microscopy images of mtSOX showed that superoxide production was gradually increased by VEM. Representative data of three independent experiments. (F) VEM significantly increased the relative change in fluorescence intensity of mtSOX at 24 h (**$p < 0.01$; unpaired t-test) ($n = 4$). Data are presented as the mean ± standard deviation. $p < 0.05$ indicates statistical significance. NS, not significant.

in the number and enlargement of lysosomes observed in the TEM images (Figure 1F). This heightened LysoTracker fluorescence intensity induced by VEM may also indicate a potential impact on the acidification of the lysosomes themselves, suggesting the impairment of lysosomal function and the possibility of autophagy malfunction.

The difficulty in distinguishing mitochondria in the TEM images of VEM-treated cells (Figure 1F) may have been due to the increase in the number and size of lysosomes and decrease in mitochondrial size, as no significant changes in mitochondrial volume were observed after VEM or BAFA1 exposure. Bai et al. confirmed that VEM induces mitochondrial dysfunction [15]. The mitochondrial morphological abnormalities observed in this study (Figure 1F) suggest mitochondrial damage [36, 37]. The superoxide-specific indicator mtSOX was used to further elucidate the effects of VEM on mitochondrial function (Figure 2D). The fluorescence intensity of mtSOX increased over time immediately after VEM exposure (Figure 2E) and was significantly higher than that of the control at 24 h (Figure 2D,F).

3.3 | BAFA1 Inhibits Lysosome Acidification but Does Not Alleviate VEM Cytotoxicity in Human RPTECs

Figure 3A shows representative images of LysoTracker staining in RPTECs 24 h after cotreatment with VEM and BAFA1. BAFA1 inhibited the VEM-induced increase in lysosomal fluorescence intensity at 24 h (Figure 3B). These results indicated that BAFA1 inhibited lysosome acidification, but it was unclear whether it also reduced lysosome accumulation and enlargement. Cotreatment with BAFA1 neither improved nor worsened the decrease in cell viability caused by VEM treatment (Figure 3C). Interestingly, BAFA1 itself significantly decreased the viability of RPTECs, suggesting that BAFA1 was cytotoxic to

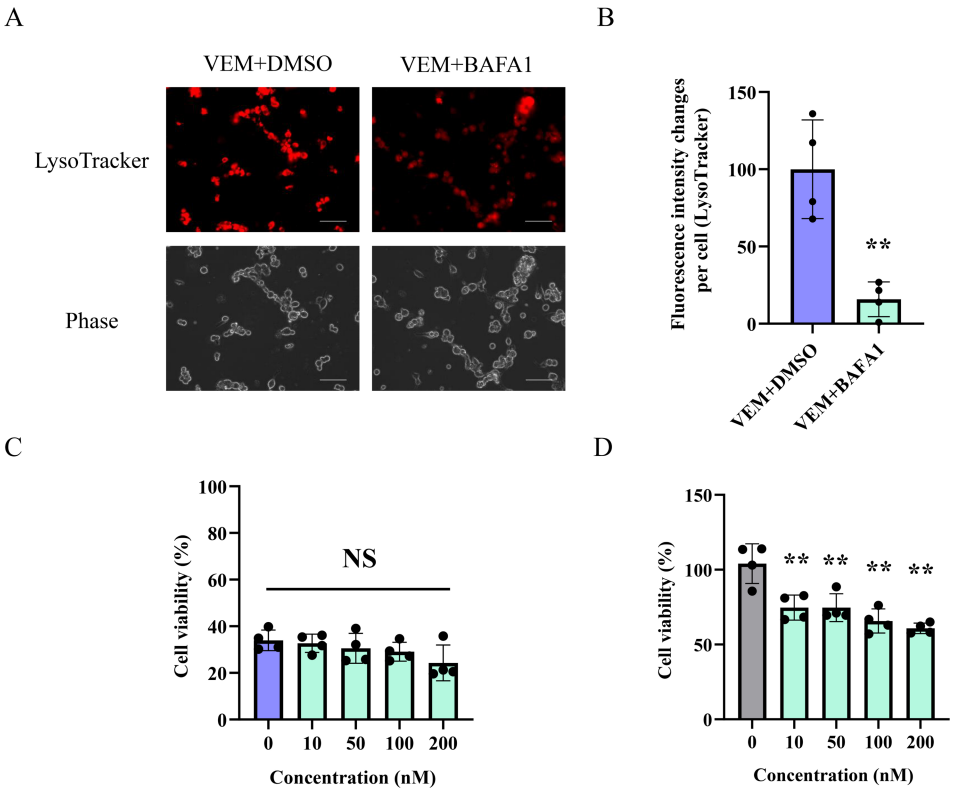

FIGURE 3 | BAFA1 inhibits lysosome acidification but does not alleviate VEM cytotoxicity in human RPTECs. (A) LysoTracker fluorescence microscopy showed that fluorescence intensity increased by VEM was suppressed by cotreatment with 50-μM BAFA1. Representative images of four independent experiments. Images captured using a 20× objective lens. Scale bar, 100 μm. (B) Cotreatment with VEM and BAFA1 significantly decreased relative changes in fluorescence intensity of LysoTracker per cell at 24 h (**$p < 0.01$; unpaired *t*-test) ($n = 4$). (C) BAFA1 did not affect cell viability decreased by VEM. (D) BAFA1 itself significantly decreased cell viability of RPTECs (**$p < 0.01$ compared with 0-μM BAFA1; one-way ANOVA with Dunnett's multiple comparison test) ($n = 4$). Data are presented as the mean ± standard deviation. $p < 0.05$ indicates statistical significance. NS, not significant.

RPTECs (Figure 3D). The results that cotreatment with BAFA1 did not exhibit additional cytotoxicity in RPTECs treated with VEM suggest that there may be some overlap in the cytotoxic mechanisms of BAFA1 and VEM.

3.4 | XJB-5-131 Alleviates VEM-Induced Superoxide Production and Cytotoxicity in Human RPTECs

XJB-5-131 is a mitochondrial targeting nitroxide with a high affinity for RPTECs [39, 40]. Figure 4A shows the representative images of mtSOX in RPTECs 24 h after cotreatment with VEM and XJB-5-131. Additionally, Figure 4B shows the representative time-course changes in the fluorescence intensity of mtSOX after cotreatment with VEM and XJB-5-131. These results suggested that cotreatment with XJB-5-131 inhibited the time-dependent increase in the fluorescence intensity of mtSOX caused by VEM (Figure 4B). Furthermore, cotreatment with XJB-5-131 reduced the fluorescence intensity of mtSOX compared with that of the control at 24 h (Figure 4C). We then evaluated the effect of inhibiting VEM-induced superoxide production by XJB-5-131 on VEM-induced cytotoxicity in RPTECs. Cotreatment with XJB-5-131 inhibited the decrease in cell viability of RPTEC caused by 50-μM VEM for 24 h and moderately improved cell viability in a concentration-dependent manner (Figure 4D). Evaluation of the cytotoxicity of XJB-5-131 showed that 10-μM XJB-5-131 did not decrease RPTEC viability (Figure 4E). Therefore, these results suggested that the inhibition of VEM-induced superoxide production by XJB-5-131 partially reduced the cytotoxicity of VEM in RPTECs.

4 | Discussion

In this study, we exposed human RPTECs to VEM and evaluated their intracellular ultrastructure and function, elucidating the mechanism of VEM-induced renal tubular toxicity. VEM exposure for 24 h damaged RPTECs and reduced their proliferation; however, typical cell death was not observed. Electron and fluorescence microscopy revealed the accumulation and enlargement of vacuoles derived from lysosomes following VEM exposure. Although this study could not conclusively determine whether this phenomenon is directly involved in VEM-induced cytotoxicity, our results suggest that the enhanced superoxide production in mitochondria caused by VEM is partially involved in the mechanism of renal tubular toxicity.

Previous studies have not described the type of cell death induced by VEM [15]. In the present study, TEM imaging of RPTECs exposed to VEM for 24 h did not reveal typical apoptosis

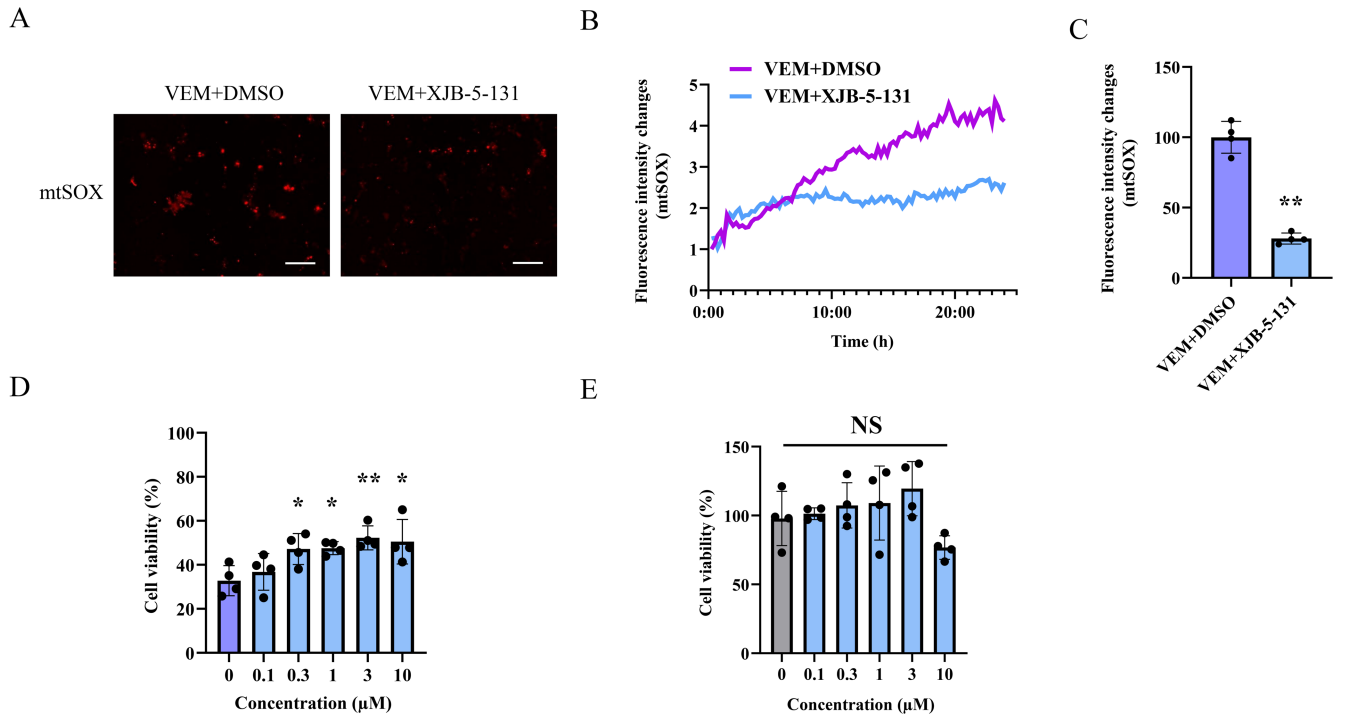

FIGURE 4 | XJB-5-131 alleviates VEM-induced superoxide production and cytotoxicity in human RPTECs. (A) mtSOX fluorescence microscopy showed that the fluorescence intensity increased by VEM was suppressed by cotreatment with 3-μM XJB-5-131. Images captured using a 10× objective lens. Scale bar, 200 μm. (B) Time-lapse fluorescence microscopy images of mtSOX showed superoxide production suppressed by cotreatment with VEM and 3-μM XJB-5-131. Representative data of three independent experiments. (C) Cotreatment with VEM and 3-μM XJB-5-131 significantly decreased relative changes in fluorescence intensity of mtSOX at 24 h (**$p < 0.01$; Welch's t-test) ($n = 4$). (D) XJB-5-131 significantly improved cell viability decreased by VEM (*$p < 0.05$, **$p < 0.01$ compared with VEM + 0-μM XJB-5-131; one-way ANOVA with Dunnett's multiple comparison test) ($n = 4$). (E) XJB-5-131 itself did not affect cell viability of RPTEC ($n = 4$). Data are presented as the mean ± standard deviation. $p < 0.05$ indicates statistical significance. NS, not significant.

or necrosis with cell membrane rupture, as observed after cisplatin exposure. Despite the absence of typical cell death, VEM reduced cell viability, increased LDH release and elevated the levels of proximal tubular injury markers and inflammatory cytokines, which are indicative of cell damage and decreased cell proliferation. The experimental conditions of this study, the use of cultured cells and different VEM exposure times, differed from those of previous research [15]; therefore, further studies need to be conducted under varying experimental conditions to fully understand the morphology of VEM-induced renal tubular cell death.

Dysfunctional lysosomes were observed in RPTECs damaged by VEM. TEM analysis revealed the accumulation and enlargement of vacuoles, presumed to be derived from lysosomes owing to their content of cellular debris and evaluation with LysoTracker. Similar expanded vacuoles have been observed in abemaciclib-induced atypical cell death of cancer cells [35]. However, unlike the study by Hino et al., in which blocking abemaciclib-induced vacuole formation with BAFA1 rescued cancer cells from cell death [35], our study found that BAFA1 did not affect VEM-induced cytotoxicity. This suggests that the vacuoles observed in our study differed from those induced by abemaciclib [35]. BAFA1 is known to inhibit lysosomal acidification and autophagosome-lysosome fusion by blocking vacuolar-type ATPase [38]. Our results, consistent with that of Martins et al. [41], showed that cotreatment with BAFA1 and VEM did not affect VEM cytotoxicity. However, the accumulation of dysfunctional lysosomes observed following VEM treatment alone suggests that VEM itself may inhibit the autophagy flux [38]. Thus, the involvement of autophagy in VEM-induced cytotoxicity remains unclear, necessitating further research to determine whether the lysosomal dysfunction observed with VEM is a secondary consequence of an earlier impairment.

VEM induced mitochondrial dysfunction and superoxide production in RPTECs. MitoTracker evaluation showed no change in the total mitochondrial volume, but TEM images revealed less visible and smaller mitochondria 24 h after VEM treatment. Changes in mitochondrial size are associated with fission and fusion processes. Mitochondrial fission has been observed in ischemia- and cisplatin-induced renal injury, suggesting mitochondrial damage and subsequent tubular damage or cell death [36, 37]. Our TEM findings indicated that VEM induced mitochondrial damage and subsequent tubular damage. Additionally, mtSOX evaluation showed that VEM treatment enhanced superoxide production. Superoxide, the first reactive oxygen species produced in mitochondria, can trigger inflammation and cell death [36]. Bai et al. demonstrated that VEM inhibits the mitochondrial respiratory chain and decreases ATP production [15]. These findings supported our conclusion that VEM induces mitochondrial dysfunction. Furthermore, the mitochondria-specific antioxidant XJB-5-131 moderately improved the viability of VEM-treated RPTECs, suggesting that superoxide is partially involved in VEM-induced renal tubular toxicity. Interestingly, Hino et al. also demonstrated that the

antioxidant *N*-acetyl-L-cysteine has a mild effect in suppressing abemaciclib-induced atypical cell death [35].

Reduction in VEM-induced FECH activity has also been reported to partially contribute to renal tubular toxicity [15]. Several studies have indicated that superoxide levels decrease FECH expression and activity [42–44]. Although these previous and current findings provide credible information regarding the association between decreased FECH activity and enhanced superoxide production in VEM-induced renal tubular toxicity, whether these phenomena are independent or related requires further investigation.

To the best of our knowledge, targets other than FECH have not been identified for VEM-induced tubular toxicity. Identifying target molecules common to drug-induced kidney injury would be helpful for its prevention and treatment. Previous studies have identified various compounds, apart from VEM, that inhibit FECH [45–47]. Off-target effects of VEM other than FECH have also been reported [48–53]. Further research is required to elucidate the relationship between drug-induced kidney injury and FECH, as well as the relationship between off-target effects other than FECH and VEM-induced renal tubular toxicity.

The present study provides evidence of mitochondrial and lysosomal abnormalities in damaged RPTECs caused by VEM. Moreover, this study is the first to demonstrate that superoxide partially contributes to the mechanism of VEM-induced renal tubular toxicity. These findings may serve as important cues for a comprehensive understanding of the mechanisms underlying VEM-induced renal tubular toxicity.

Acknowledgements

We would like to thank Editage (www.editage.com) for English language editing.

Conflicts of Interest

The authors declare no conflicts of interest.

Data Availability Statement

The data that support the findings of this study are available from the corresponding author upon reasonable request.

References

1. M. H. Rosner and M. A. Perazella, "Acute Kidney Injury in Patients With Cancer," *New England Journal of Medicine* 376, no. 18 (2017): 1770–1781, https://doi.org/10.1056/NEJMra1613984.

2. H. Izzedine and M. A. Perazella, "Anticancer Drug-Induced Acute Kidney Injury," *Kidney International Reports* 2, no. 4 (2017): 504–514, https://doi.org/10.1016/j.ekir.2017.02.008.

3. M. A. Perazella and H. Izzedine, "New Drug Toxicities in the Onco-Nephrology World," *Kidney International* 87, no. 5 (2015): 909–917, https://doi.org/10.1038/ki.2015.30.

4. M. A. Perazella, "Onco-Nephrology: Renal Toxicities of Chemotherapeutic Agents," *Clinical Journal of the American Society of Nephrology* 7, no. 10 (2012): 1713–1721, https://doi.org/10.2215/CJN.02780312.

5. H. Maeda, A. Hara, M. Ofuchi, R. Shingai, T. Misumi, and Y. Murai, "Trends in Oncology Drug Lags in Japan From 2001 to 2020: A Cross-Sectional Study," *Clinical and Translational Science* 16, no. 12 (2023): 2665–2674, https://doi.org/10.1111/cts.13660.

6. S. Wang, Q. Yang, L. Deng, et al., "An Overview of Cancer Drugs Approved Through Expedited Approval Programs and Orphan Medicine Designation Globally Between 2011 and 2020," *Drug Discovery Today* 27, no. 5 (2022): 1236–1250, https://doi.org/10.1016/j.drudis.2021.12.021.

7. K. D. Jhaveri, R. Wanchoo, V. Sakhiya, D. W. Ross, and S. Fishbane, "Adverse Renal Effects of Novel Molecular Oncologic Targeted Therapies: A Narrative Review," *Kidney International Reports* 2, no. 1 (2016): 108–123, https://doi.org/10.1016/j.ekir.2016.09.055.

8. P. B. Chapman, A. Hauschild, C. Robert, et al., "Improved Survival With Vemurafenib in Melanoma With BRAF V600E Mutation," *New England Journal of Medicine* 364, no. 26 (2011): 2507–2516, https://doi.org/10.1056/NEJMoa1103782.

9. J. Larkin, P. A. Ascierto, B. Dréno, et al., "Combined Vemurafenib and Cobimetinib in BRAF-Mutated Melanoma," *New England Journal of Medicine* 371 (2014): 1867–1876, https://doi.org/10.1056/NEJMoa1408868.

10. V. Launay-Vacher, S. Zimner-Rapuch, N. Poulalhon, et al., "Acute Renal Failure Associated With the New BRAF Inhibitor Vemurafenib: A Case Series of 8 Patients," *Cancer* 120, no. 14 (2014): 2158–2163, https://doi.org/10.1002/cncr.28709.

11. K. D. Jhaveri, V. Sakhiya, and S. Fishbane, "Nephrotoxicity of the BRAF Inhibitors Vemurafenib and Dabrafenib," *JAMA Oncology* 1, no. 8 (2015): 1133–1134, https://doi.org/10.1001/jamaoncol.2015.1713.

12. R. Wanchoo, K. D. Jhaveri, G. Deray, and V. Launay-Vacher, "Renal Effects of BRAF Inhibitors: A Systematic Review by the Cancer and the Kidney International Network," *Clinical Kidney Journal* 9, no. 2 (2016): 245–251, https://doi.org/10.1093/ckj/sfv149.

13. C. Teuma, M. Perier-Muzet, S. Pelletier, et al., "New Insights Into Renal Toxicity of the B-RAF Inhibitor, Vemurafenib, in Patients With Metastatic Melanoma," *Cancer Chemotherapy and Pharmacology* 78 (2016): 419–426, https://doi.org/10.1007/s00280-016-3086-7.

14. C. Hurabielle, E. Pillebout, T. Stehlé, et al., "Mechanisms Underpinning Increased Plasma Creatinine Levels in Patients Receiving Vemurafenib for Advanced Melanoma," *PLoS ONE* 11 (2016): e0149873, https://doi.org/10.1371/journal.pone.0149873.

15. Y. Bai, J. Y. Kim, B. Bisunke, et al., "Kidney Toxicity of the BRAF-Kinase Inhibitor Vemurafenib Is Driven by Off-Target Ferrochelatase Inhibition," *Kidney International* 100, no. 6 (2021): 1214–1226, https://doi.org/10.1016/j.kint.2021.08.022.

16. M. Balwani, H. Naik, K. E. Anderson, et al., "Clinical, Biochemical, and Genetic Characterization of North American Patients With Erythropoietic Protoporphyria and X-Linked Protoporphyria," *JAMA Dermatology* 153, no. 8 (2017): 789–796, https://doi.org/10.1001/jamadermatol.2017.1557.

17. J. Bloomer, C. Bruzzone, L. Zhu, Y. Scarlett, S. Magness, and D. Brenner, "Molecular Defects in Ferrochelatase in Patients With Protoporphyria Requiring Liver Transplantation," *Journal of Clinical Investigation* 102 (1998): 107–114, https://doi.org/10.1172/JCI1347.

18. Y. Nakahashi, H. Fujita, S. Taketani, N. Ishida, A. Kappas, and S. Sassa, "The Molecular Defect of Ferrochelatase in a Patient With Erythropoietic Protoporphyria," *Proceedings of the National Academy of Sciences of the United States of America* 89, no. 1 (1992): 281–285, https://doi.org/10.1073/pnas.89.1.281.

19. M. J. Tracz, J. Alam, and K. A. Nath, "Physiology and Pathophysiology of Heme: Implications for Kidney Disease," *Journal of the American Society of Nephrology* 18, no. 2 (2007): 414–420, https://doi.org/10.1681/ASN.2006080894.

20. J. S. Woods, "Regulation of Porphyrin and Heme Metabolism in the Kidney," *Seminars in Hematology* 25, no. 4 (1988): 336–348.

21. N. Pallet, A. Karras, E. Thervet, L. Gouya, Z. Karim, and H. Puy, "Porphyria and Kidney Diseases," *Clinical Kidney Journal* 11, no. 2 (2018): 191–197, https://doi.org/10.1093/ckj/sfx146.

22. N. Pallet, A. Karras, E. Thervet, et al., "High Prevalence of and Potential Mechanisms for Chronic Kidney Disease in Patients With Acute Intermittent Porphyria," *Kidney International* 88, no. 2 (2015): 386–395, https://doi.org/10.1038/ki.2015.97.

23. P. Tveden-Nyborg, T. K. Bergmann, N. Jessen, U. Simonsen, and J. Lykkesfeldt, "BCPT 2023 Policy for Experimental and Clinical Studies," *Basic & Clinical Pharmacology & Toxicology* 133, no. 4 (2023): 391–396, https://doi.org/10.1111/bcpt.13944.

24. A. Sanagawa, Y. Hotta, N. Mori, et al., "BRAF/MEK Inhibitor-Associated Nephrotoxicity in a Real-World Setting and Human Kidney Cells," *Anti-Cancer Drugs* 32 (2021): 1076–1083, https://doi.org/10.1097/CAD.0000000000001106.

25. A. Sanagawa, Y. Hotta, R. Sezaki, et al., "Effect of Replicative Senescence on the Expression and Function of Transporters in Human Proximal Renal Tubular Epithelial Cells," *Biological & Pharmaceutical Bulletin* 45, no. 11 (2022): 1636–1643, https://doi.org/10.1248/bpb.b22-00322.

26. B. D. Humphreys, F. Xu, V. Sabbisetti, et al., "Chronic Epithelial Kidney Injury Molecule-1 Expression Causes Murine Kidney Fibrosis," *Journal of Clinical Investigation* 123 (2013): 4023–4035, https://doi.org/10.1172/JCI45361.

27. B. A. Yard, M. R. Daha, M. Kooymans-Couthino, et al., "IL-1 Alpha Stimulated TNF Alpha Production by Cultured Human Proximal Tubular Epithelial Cells," *Kidney International* 42, no. 2 (1992): 383–389, https://doi.org/10.1038/ki.1992.299.

28. S. Tang, J. C. Leung, K. Abe, et al., "Albumin Stimulates Interleukin-8 Expression in Proximal Tubular Epithelial Cells In Vitro and In Vivo," *Journal of Clinical Investigation* 111 (2003): 515–527, https://doi.org/10.1172/JCI16079.

29. T. Salti, K. Khazim, R. Haddad, S. Campisi-Pinto, G. Bar-Sela, and I. Cohen, "Glucose Induces IL-1α-Dependent Inflammation and Extracellular Matrix Proteins Expression and Deposition in Renal Tubular Epithelial Cells in Diabetic Kidney Disease," *Frontiers in Immunology* 11 (2020): 1270, https://doi.org/10.3389/fimmu.2020.01270.

30. Y. Tanaka, S. Kume, M. Chin-Kanasaki, et al., "Renoprotective Effect of DPP-4 Inhibitors Against Free Fatty Acid-Bound Albumin-Induced Renal Proximal Tubular Cell Injury," *Biochemical and Biophysical Research Communications* 470, no. 3 (2016): 539–545, https://doi.org/10.1016/j.bbrc.2016.01.109.

31. H. B. Nguyen, T. Q. Thai, S. Saitoh, et al., "Conductive Resins Improve Charging and Resolution of Acquired Images in Electron Microscopic Volume Imaging," *Scientific Reports* 6 (2016): 23721, https://doi.org/10.1038/srep23721.

32. T. Hanaichi, T. Sato, T. Iwamoto, J. Malavasi-Yamashiro, M. Hoshino, and N. Mizuno, "A Stable Lead by Modification of Sato's Method," *Journal of Electron Microscopy* 35, no. 3 (1986): 304–306, https://doi.org/10.1093/oxfordjournals.jmicro.a050582.

33. R. Muko, H. Matsuda, M. A. Oikawa, et al., "Histidine-Rich Glycoprotein Functions as a Dual Regulator of Neutrophil Activity in Horses," *Journal of Equine Veterinary Science* 102 (2021): 103620, https://doi.org/10.1016/j.jevs.2021.103620.

34. H. T. Sakurai, H. Iwashita, S. Arakawa, et al., "Development of Small Fluorescent Probes for the Analysis of Autophagy Kinetics," *iScience* 26, no. 7 (2023): 107218, https://doi.org/10.1016/j.isci.2023.107218.

35. H. Hino, N. Iriyama, H. Kokuba, et al., "Abemaciclib Induces Atypical Cell Death in Cancer Cells Characterized by Formation of Cytoplasmic Vacuoles Derived From Lysosomes," *Cancer Science* 111, no. 6 (2020): 2132–2145, https://doi.org/10.1111/cas.14419.

36. T. Doke and K. Susztak, "The Multifaceted Role of Kidney Tubule Mitochondrial Dysfunction in Kidney Disease Development," *Trends in Cell Biology* 32, no. 10 (2022): 841–853, https://doi.org/10.1016/j.tcb.2022.03.012.

37. R. Huang, C. Zhang, Z. Xiang, T. Lin, J. Ling, and H. Hu, "Role of Mitochondria in Renal Ischemia-Reperfusion Injury," *FEBS Journal* 291, no. 24 (2024): 5365–5378, https://doi.org/10.1111/febs.17130.

38. D. J. Klionsky, Z. Elazar, P. O. Seglen, and D. C. Rubinsztein, "Does Bafilomycin A1 Block the Fusion of Autophagosomes With Lysosomes?," *Autophagy* 4, no. 7 (2008): 849–850, https://doi.org/10.4161/auto.6845.

39. T. Krainz, M. M. Gaschler, C. Lim, J. R. Sacher, B. R. Stockwell, and P. Wipf, "A Mitochondrial-Targeted Nitroxide Is a Potent Inhibitor of Ferroptosis," *ACS Central Science* 2, no. 9 (2016): 653–659, https://doi.org/10.1021/acscentsci.6b00199.

40. Z. Zhao, J. Wu, H. Xu, et al., "XJB-5-131 Inhibited Ferroptosis in Tubular Epithelial Cells After Ischemia-Reperfusion Injury," *Cell Death & Disease* 11 (2020): 629, https://doi.org/10.1038/s41419-020-02871-6.

41. W. K. Martins, N. F. Santos, C. S. Rocha, et al., "Parallel Damage in Mitochondria and Lysosomes Is an Efficient Way to Photoinduce Cell Death," *Autophagy* 15, no. 2 (2019): 259–279, https://doi.org/10.1080/15548627.2018.1515609.

42. A. J. Case, J. M. Madsen, D. G. Motto, D. K. Meyerholz, and F. E. Domann, "Manganese Superoxide Dismutase Depletion in Murine Hematopoietic Stem Cells Perturbs Iron Homeostasis, Globin Switching, and Epigenetic Control in Erythrocyte Precursor Cells," *Free Radical Biology & Medicine* 56 (2013): 17–27, https://doi.org/10.1016/j.freeradbiomed.2012.11.018.

43. D. Patel, R. Alhawaj, M. R. Kelly, et al., "Potential Role of Mitochondrial Superoxide Decreasing Ferrochelatase and Heme in Coronary Artery Soluble Guanylate Cyclase Depletion by Angiotensin II," *American Journal of Physiology. Heart and Circulatory Physiology* 310, no. 11 (2016): H1439–H1447, https://doi.org/10.1152/ajpheart.00859.2015.

44. H. Yu, N. Alruwaili, M. R. Kelly, et al., "Endothelin-1 Depletion of Cartilage Oligomeric Matrix Protein Modulates Pulmonary Artery Superoxide and Iron Metabolism-Associated Mitochondrial Heme Biosynthesis," *American Journal of Physiology. Lung Cellular and Molecular Physiology* 323, no. 4 (2022): L400–L409, https://doi.org/10.1152/ajplung.00534.2020.

45. M. M. Savitski, F. B. Reinhard, H. Franken, et al., "Tracking Cancer Drugs in Living Cells by Thermal Profiling of the Proteome," *Science* 346 (2014): 1255784, https://doi.org/10.1126/science.1255784.

46. S. Klaeger, B. Gohlke, J. Perrin, et al., "Chemical Proteomics Reveals Ferrochelatase as a Common Off-Target of Kinase Inhibitors," *ACS Chemical Biology* 11, no. 5 (2016): 1245–1254, https://doi.org/10.1021/acschembio.5b01063.

47. R. Yamada and M. Yanagita, "Unexpected Cause of Vemurafenib-Induced Nephrotoxicity: Ferrochelatase," *Kidney International* 100 (2021): 1158–1160, https://doi.org/10.1016/j.kint.2021.09.010.

48. E. Madej, A. A. Brożyna, A. Adamczyk, et al., "Vemurafenib and Dabrafenib Downregulates RIPK4 Level," *Cancers (Basel)* 15 (2023): 918, https://doi.org/10.3390/cancers15030918.

49. B. Pfaffenrot, P. Klövekorn, M. Juchum, et al., "Design and Synthesis of 1H-pyrazolo[3,4-b]pyridines Targeting Mitogen-Activated Protein Kinase Kinase 4 (MKK4)—A Promising Target for Liver Regeneration," *European Journal of Medicinal Chemistry* 218 (2021): 113371, https://doi.org/10.1016/j.ejmech.2021.113371.

50. J. Perrin, T. Werner, N. Kurzawa, et al., "Identifying Drug Targets in Tissues and Whole Blood With Thermal-Shift Profiling," *Nature Biotechnology* 38 (2020): 303–308, https://doi.org/10.1038/s41587-019-0388-4.

51. S. Mathea, K. R. Abdul Azeez, E. Salah, et al., "Structure of the Human Protein Kinase ZAK in Complex With Vemurafenib," *ACS Chemical Biology* 11, no. 6 (2016): 1595–1602, https://doi.org/10.1021/acschembio.6b00043.

52. H. Vin, S. S. Ojeda, G. Ching, et al., "BRAF Inhibitors Suppress Apoptosis Through Off-Target Inhibition of JNK Signaling," *eLife* 2 (2013): e00969, https://doi.org/10.7554/eLife.00969.

53. S. Bromberger, Y. Zadorozhna, J. M. Ressler, et al., "Off-Targets of BRAF Inhibitors Disrupt Endothelial Signaling and Vascular Barrier Function," *Life Science Alliance* 5, no. 7 (2024): e202402671, https://doi.org/10.26508/lsa.202402671.